Check for updates

RESEARCH ARTICLE
Rising Stars
ADVANCED OPTICAL MATERIALS
www.advopticalmat.de

Alleviating Parasitic Back Energy Transfer Enhances Thin Film Upconversion

*Pournima Narayanan, Manchen Hu, Linda Pucurimay, Arynn O. Gallegos, Qi Zhou, Emma Belliveau, Ghada H. Ahmed, Sebastian Fernández, William Michaels, Natalia Murrietta, Vongaishe E. Mutatu, Demeng Feng, Rabeeya Hamid, Kyra M. K. Yap, Tracy H. Schloemer, Thomas F. Jaramillo, Mikhail A. Kats, and Daniel N. Congreve**

Upconversion (UC) of low-energy photons to higher-energy photons enables exciting advances in 3D printing, bioimaging, and more. Particularly, the UC of near-infrared (NIR) photons is identified as a process that can enhance photovoltaic, night vision, and anti-counterfeiting technologies. Triplet–triplet annihilation UC is especially attractive due to its low UC thresholds and broadband, tunable absorption. However, state-of-the-art NIR-to-visible solid-state UC thin films made of PbS quantum dots and rubrene are limited by 1) low absorption of NIR photons, 2) inefficient energy transfer, and 3) parasitic back transfer processes, leading to low efficiencies unsuitable for wide application. Here, a multi-layer architecture that allows for strongly absorbing UC films with improved efficiencies is proposed. 5-tetracene carboxylic acid is used as an interlayer to improve energy transfer to rubrene and alleviate parasitic back transfer leading to a factor of five improvement in efficiency. Finally, UC anti-counterfeiting is demonstrated, highlighting the film's potential for UC-facilitated technologies.

1. Introduction

Photon upconversion (UC), the process of converting low-energy photons into higher-energy photons, holds tremendous potential for various applications including photovoltaics,[1–5] night vision,[6,7] photocatalysis,[8–11] bioimaging,[12–18] anti-counterfeiting,[19–21] additive manufacturing,[22–25] and more.[26–29] The anti-Stokes shift achieved by short-wave- and near-infrared-to-visible UC is instrumental to address the bandgap limitations of silicon[2,3,6,30] and to exploit the positioning of key transparency windows in biological systems.[31–34] By absorbing sub-bandgap photons in the NIR region, UC-assisted photovoltaics have been proposed to achieve higher efficiencies beyond single-junction solar cells.[2,3,5] Additionally, the difficulty in replicating NIR-to-visible anti-Stokes shifts presents an opportunity to employ UC for anti-counterfeiting applications.[19–21]

There have been several reported mechanisms to achieve visible emission from NIR excitation, including excited-state absorption,[28,35] energy-transfer UC,[28,35] photon avalanching,[28,35,36] collective energy pooling,[37] and triplet–triplet annihilation upconversion (TTA-UC).[28,38] Various f-block elements have been deployed in nanocrystals and solids to achieve tunable, sharp, and significantly anti-Stokes-shifted emission by creating ultraviolet (UV) or visible photons from NIR photons.[28] Despite the large anti-Stokes shift achieved by these systems via f–f transitions, they are often limited in applicability due to their need for high intensities of light and narrow absorption bands.[25,27,28] UC via TTA shows particular promise for applications because it can occur relatively efficiently under lower-intensity irradiation from incoherent and broadband sources of light.[26,28,29]

In the overall TTA-UC process, two low-energy photons are absorbed and converted into one higher-energy photon. The mechanism of TTA-UC relies on two species: the sensitizer and the annihilator (see **Figure 1a**). The annihilator is an organic semiconductor (often an acene) with energetics such that two triplet-excited annihilator molecules can interact via TTA to generate one singlet-excited and one ground-state annihilator molecule.

P. Narayanan, M. Hu, L. Pucurimay, A. O. Gallegos, Q. Zhou, E. Belliveau, G. H. Ahmed, S. Fernández, W. Michaels, N. Murrietta, V. E. Mutatu, T. H. Schloemer, D. N. Congreve
Department of Electrical Engineering
Stanford University
Stanford, CA 94305, USA
E-mail: Congreve@stanford.edu

P. Narayanan
Department of Chemistry
Stanford University
Stanford, CA 94305, USA

L. Pucurimay
Department of Material Science Engineering
Stanford University
Stanford, CA 94305, USA

D. Feng, R. Hamid, M. A. Kats
Department of Electrical and Computer Engineering
University of Wisconsin – Madison
Madison, WI 53706, USA

K. M. K. Yap, T. F. Jaramillo
Department of Chemical Engineering
Stanford University
Stanford, CA 94305, USA

The ORCID identification number(s) for the author(s) of this article can be found under https://doi.org/10.1002/adom.202500252

DOI: 10.1002/adom.202500252

 © 2025 Wiley-VCH GmbH

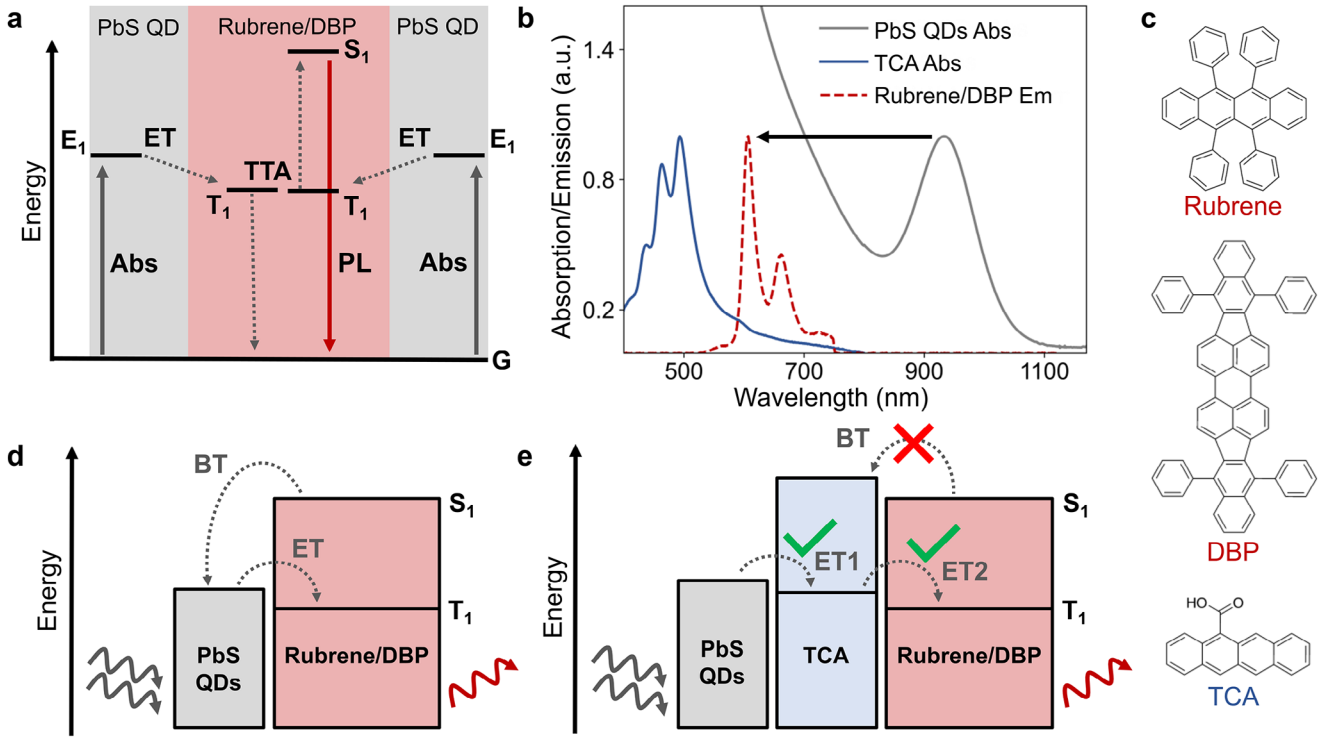

Figure 1. a) Schematic energy diagram showing the mechanism of triplet–triplet annihilation upconversion (TTA-UC). PbS QDs absorb (Abs) incident NIR light to sensitize rubrene via energy transfer (ET). Two triplet-excited rubrene molecules undergo triplet–triplet annihilation (TTA) to generate a singlet state which can emit a visible photon (PL). b) Emission spectrum of rubrene/DBP (1 vol% doping of DBP in rubrene) (dashed, red) and absorption spectra of PbS (gray) and TCA (blue). Arrow highlights the anti-Stokes shift achieved by this system. c) Molecular structures of rubrene ($S_1 = 2.25$, $T_1 = 1.14$ eV), DBP, and TCA (5-tetracene carboxylic acid, $S_1 = 2.4$ eV, $T_1 = \approx 1.3$ eV). d) Energy diagram of the traditional PbS-rubrene/DBP UC thin-film architecture with gray, dotted arrows highlighting the energy transfer processes. e) Energy diagram of our proposed thin-film architecture with an interlayer between rubrene and PbS QDs such that ET in the forward direction is maintained and parasitic back transfer (BT) is reduced to improve UC performance.

The singlet-excited annihilator molecule can then relax to the ground state by emitting a high-energy photon via photoluminescence (PL). As shown in Figure 1a, sensitizers are necessary to create triplet-excited annihilator molecules, as triplet states in organic semiconductors are typically optically inaccessible. Sensitizer species absorb light (Abs) to create an excited state (typically a singlet), which can undergo intersystem crossing (ISC) to generate a triplet which can transfer its energy to an annihilator via Dexter energy transfer (ET). There are various families of sensitizers for TTA including semiconducting quantum dots (QDs),[39–41] thermally activated delayed fluorescence molecules,[42,43] heavy metal porphyrin complexes,[38,44] and non-fullerene acceptors.[45,46]

Commercial realization of solid-state NIR-to-visible UC demands that this conversion process be highly efficient. Zhou et al. have summarized essential metrics to measure the efficiency of UC systems.[46] Here, we use external quantum efficiency (EQE) as a performance metric due to its relevance to applications like photovoltaics, night vision, and anti-counterfeiting. EQE is defined as the number of upconverted photons generated by 100 incident low-energy photons. To follow the norms adopted by the field, all EQEs in this article will be reported with a maximum possible 50% (due to the two-photons-to-one-photon nature of TTA-UC).[47]

Arguably the most well-studied annihilator for NIR-to-visible UC to date is rubrene (see Figure 1c), a tetracene derivative.[48] DBP, an organic semiconductor (see Figure 1c), is often doped into rubrene films to improve the resulting photoluminescence quantum yield (PLQY) by acting as a singlet sink to prevent triplet separation.[49,50] Rubrene has been reported to be sensitized by a wide range of materials, including organic semiconductors (Y6, ITIC-Cl),[7,45,46,51,52] semiconducting QDs (PbS, PbSe),[40,41,53–55] 2D transition metal dichalcogenides,[56,57] and heavy metal complexes (PdPc, PtTPTNP, osmium complexes, and more).[5,58–61] Despite their promising performance, most organic NIR-to-visible sensitizers are limited to excitation wavelengths below ≈1000 nm.

PbS QDs are highly appealing sensitizers due to their broad and tunable absorption spectra which can span the NIR region (750–2000 nm) through well-established synthetic control of their diameter.[62] Due to this tunability, PbS QDs have also been demonstrated as promising sensitizers in UC systems with non-rubrene annihilators.[63–65] The PbS-rubrene/DBP system has shown visible UC emission from excitations up to 1100 nm.[40] Successful solid-state NIR-to-visible UC systems employing PbS quantum dots as the sensitizer and rubrene as the annihilator (see Figure 1a,b) were reported in 2016 with EQEs under 0.0003%.[40] Since this initial demonstration, there have been

© 2025 Wiley-VCH GmbH

21951071, 0, Downloaded from https://advanced.onlinelibrary.wiley.com/doi/10.1002/adom.202500252 by Massachusetts Institute of Technolo, Wiley Online Library on [03/06/2025]. See the Terms and Conditions (https://onlinelibrary.wiley.com/terms-and-conditions) on Wiley Online Library for rules of use; OA articles are governed by the applicable Creative Commons License

reports which have improved the efficiencies of this system using mirrors[66] and cavities,[67] with champion EQEs of 0.06% reported by M. Wu, et al. in 2021 via the use of a Fabry–Perot cavity. Still, using cavities severely limits the broadband absorption, and therefore deters the application of this structure to applications such as photovoltaics, night vision, and anti-counterfeiting. Consequently, an approach at the excitonic engineering level is urgently needed to enhance the absorption and efficiency of these films.

To improve the EQEs of UC films toward realizing their potential, we pursued improvements to the various components contributing to the EQE. The EQE of the TTA-UC process can be broken down as the product of absorption and internal quantum efficiency (IQE). The IQE can be further broken down as the product of the efficiencies of energy transfer (φ_{ET}), TTA (φ_{TTA}), and photoluminescence (φ_{PL}) (see Equation (1)).[26,47] As shown in Figure 1d, efficient energy transfer (ET) from PbS QDs to rubrene is essential to maximize the triplet density in rubrene. This energy transfer in the forward direction (PbS QDs → rubrene) is of the Dexter type, that is, the energy transfer rate is exponentially dependent on the distance between the donor (PbS QDs) and acceptor (rubrene).[41,54,55,68–72] The insulating organic ligand shell (typically, oleic acid) adhered to the PbS QDs is known to hinder the ET efficiency due to increased spatial distance between the donor and acceptor.[41,73] This issue has been commonly overcome through the use of shorter ligands or extractor/mediator ligands on the QDs.[41,69,74–78]

$$\mathrm{EQE} = \varphi_A \times \mathrm{IQE} = \varphi_A \times \varphi_{ET} \times \varphi_{TTA} \times \left(1 - \varphi_{BT}\right) \times \varphi_{PL} \quad (1)$$

However, another major loss mechanism has been identified as a source of low efficiencies for solid-state UC beyond ET from the PbS QD to rubrene.[54,55,70–73,79–81] This loss mechanism involves parasitic energy back transfer (BT) from the rubrene singlet to the PbS QDs, as shown in Figure 1d. This BT process (rubrene singlet → PbS QDs) is a Förster resonance energy transfer (FRET) process which is exacerbated by high acceptor (PbS QD) concentrations leading to a severe drop in IQE for thicker PbS films deposited from solutions with concentrations beyond 5–10 mg mL^{-1}.[54,55,70–73,79–81] Therefore, traditional PbS QD/rubrene solid-state films report 1–2 monolayer thin PbS films with low absorptions on the order of 0.1–0.5% (excluding examples employing cavities).[40,73,82] Thus far, this low absorption has presented a bottleneck to high EQEs in QD-based solid-state TTA-UC.

The aforementioned forward (ET) and backward (BT) energy transfer processes present a paradoxical simultaneous need for proximity and distance between the sensitizer and annihilator to maximize UC EQEs. To address this challenge, we propose the introduction of an intermediate triplet-diffusing, FRET-blocking organic layer between the PbS QDs and rubrene layers (see Figure 1e). We hypothesize that the introduction of some optimal thickness of an organic semiconductor would improve EQEs by reducing the BT process. This ideal interlayer would possess a triplet energy level between that of rubrene ($T_1 = 1.14$ eV)[83] and the PbS QD bandgap (≈1.2 eV) while possessing a singlet energy level higher than that of rubrene ($S_1 = 2.25$ eV).[83] As shown in Figure 1e, this proposed thin-film architecture prevents the parasitic BT by acting as an uphill energetic barrier while maintaining the triplet energy flow to the rubrene through downhill energy transfer processes (ET1, ET2).[70,72,79,80]

Here, we report the use of 5-tetracene carboxylic acid (TCA, $S_1 = 2.4$ eV, $T_1 = \approx 1.3$ eV, see Figure 1e)[84] as an interlayer to improve NIR-to-visible solid-state UC. In addition to improvements in triplet extraction ($\varphi_{ET1/ET}$) efficiencies from PbS, we report improvements in BT alleviation (i.e., reduction in φ_{BT}) using this interlayer. We report significant improvements in EQE, particularly for thicker PbS films, and systematically identify the cause of the improvement in EQE. Finally, we demonstrate the application of this novel architecture in anti-counterfeiting by depositing a patterned TCA interlayer to create intricate images under diffuse NIR irradiation.

2. Results and Discussion

We fabricated the traditional NIR-to-visible UC films (see Figure 1d) by spin coating PbS QDs from toluene on cleaned glass substrates followed by annealing at 70 °C and thermal co-evaporation of ≈64 nm (optimized for our UC stack) of 1 vol% DBP in rubrene on top. For our novel thin-film architecture (Figure 1e), TCA was spin-coated on top of the PbS QD film before annealing and thermal co-evaporation of ≈64 nm of rubrene/DBP. All UC films were encapsulated with glass slides using UV-curing epoxy glue to prevent oxygen ingress. These UC films were excited using an 808 nm laser to observe UC from rubrene/DBP (550–750 nm emission) through a 750 nm short-pass filter (see UC emission spectrum of rubrene/DBP in Figure 1b). See the Experimental Section for further details on the UC photoluminescence measurements.

To study the UC performance, we measured the EQEs using the EQE calculation method reported by Izawa, et al.[45] and Hu, et al.[51] (see the Experimental Section for more details). We varied the thickness of the TCA by spin-coating solutions with varying concentrations of TCA in acetonitrile (1–6 mM, see Figure S8, Supporting Information for TCA optimization). Additionally, we tuned the PbS thickness by varying the PbS solution concentration between 5 and 50 mg mL^{-1} to deposit films that absorb between 0.3 and 6.2% of the incident 808 nm laser (see Notes S1,S2, Supporting Information for percent absorption calculations). As shown by the orange trace in **Figure 2a**, there was a steady decline in EQE for the control films with increasing PbS thickness (no TCA). We believe this drop in performance is from two factors: parasitic back transfer of singlets and poor inter-QD energy transfer. While thicker PbS films are expected to absorb more NIR photons, they also suffer from more parasitic BT of singlet excitons from rubrene/DBP due to a higher concentration of PbS QD acceptors. Additionally, the energy transfer between QDs is limited due to the insulating shell created by the oleic acid ligands. This organic shell limits the diffusion of excitons to the interface due to competing non-radiative processes, especially in thicker PbS films. So far, this decline in EQE with increasing PbS thickness has presented a crucial bottleneck to unlocking higher EQEs in this system.

Upon introduction of the optimal 3 mM TCA layer between PbS and rubrene/DBP, we observe a sharp EQE increase at all PbS film thicknesses. Excitingly, we achieved the highest EQE in our experiments for the thickest PbS films (50 mg mL^{-1}) allowing an absorption up to 6.2% of incident 808 nm light without

© 2025 Wiley-VCH GmbH

21951071, 0, Downloaded from https://advanced.onlinelibrary.wiley.com/doi/10.1002/adom.202500252 by Massachusetts Institute of Technolo, Wiley Online Library on [03/06/2025]. See the Terms and Conditions (https://onlinelibrary.wiley.com/terms-and-conditions) on Wiley Online Library for rules of use; OA articles are governed by the applicable Creative Commons License

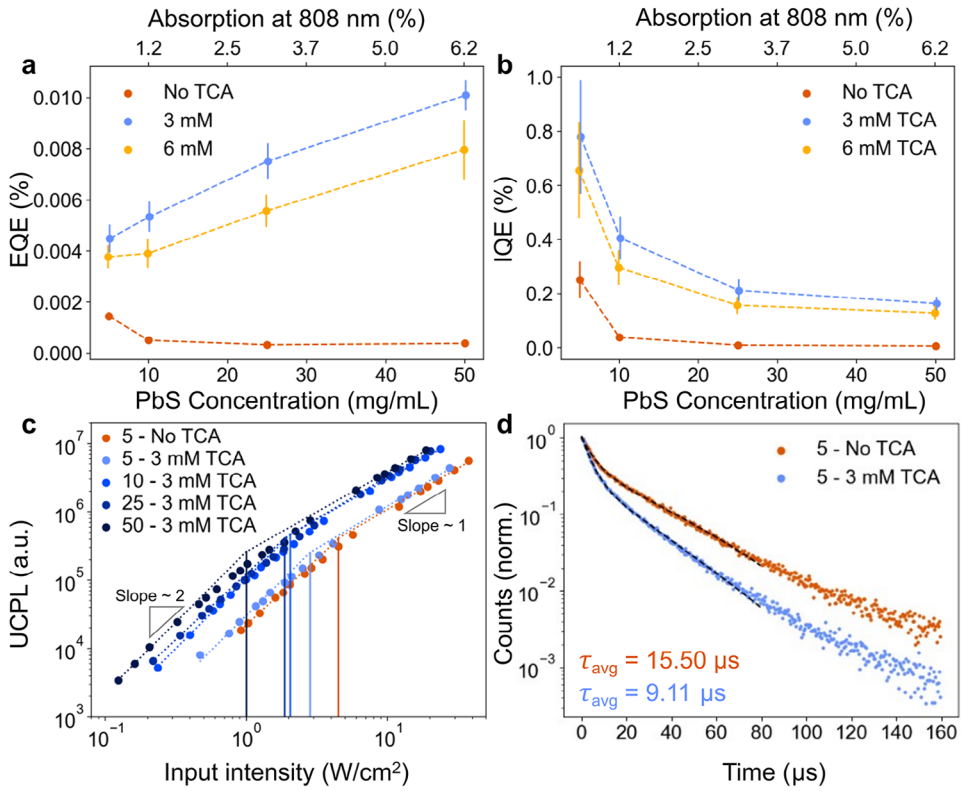

Figure 2. a) Absolute external quantum efficiencies (EQEs) and b) internal quantum efficiencies (IQEs) of UC thin films with varying TCA (3 and 6 mM), PbS concentrations (5, 10, 25, and 50 mg mL^{-1}), and percent absorption at 808 nm. Control films without TCA are shown in orange. Note: dashed lines are used only to highlight the trends with varying PbS concentrations. c) UC power dependence used to calculate the UC threshold intensities of 5 mg mL^{-1} PbS QD-based films with and without TCA (3 mM). Threshold intensities (bottom right) and slopes of linear and quadratic regimes are reported in Figure S10 and Table S1 (Supporting Information). d) Time-resolved UC photoluminescence (TRUCPL) decay curves of 5 mg mL^{-1} PbS QD-based films with and without TCA (3 mM). Decay curves for 10, 25, and 50 mg mL^{-1} PbS with 3 mM TCA are reported in Figure S11 and Table S2 (Supporting Information).

the use of cavities or mirrors (Figure 2a). We hypothesize that the massive improvements in EQE originate from 1) an improvement in energy transfer from PbS QDs, and 2) alleviated BT from rubrene/DBP to PbS QDs (see below). Based on atomic force microscopy (AFM) measurements, we determined the thickness of 3 mM TCA to be ≈10 nm (see Figures S3,S4, Supporting Information). This thickness of 3 mM TCA and the higher singlet energy level of TCA support our hypothesis that TCA alleviates FRET-based energy BT from rubrene/DBP to PbS QDs (φ_{BT}) (see Figure 1e). Additionally, the triplet level of TCA lies near the PbS bandgap and above the rubrene triplet, facilitating the energy transfer in the forward direction.

Interestingly, upon increasing the thickness of TCA to ≈19 nm by spin coating a higher concentration of 6 mM TCA, we observed a decline in EQE relative to the optimal 3 mM TCA. While the thicker TCA layer would prevent back-FRET energy transfer further, the triplets within the TCA now face non-radiative recombination pathways before reaching the TCA-rubrene/DBP interface (i.e., φ_{BT} decreases, φ_{ET2} also faces a drop with thicker TCA films).

Since EQE is defined as the product of percent absorption and IQE (see Equation (2)), the IQE can be calculated as the EQE divided by the percent absorption. When we normalized the EQEs with percent absorption to obtain IQEs, we observed that the IQE remains highest for 5 mg mL^{-1} PbS QDs (see Figure 2b) with or without TCA. At increasing PbS film thicknesses, the IQE drops. However, for UC films with thicker PbS films, the IQE improvement achieved by the incorporation of TCA is extremely high (27× improvement for 50 mg mL^{-1} PbS from (0.006 ± 0.001)% to (0.163 ± 0.026)%). For applications like photovoltaics and night vision, high absorption and high IQE are both required, yet thus far a rise in absorption has been related to a significant drop in IQE of UC films. This work presents a large stride toward the goal of simultaneous maximization of IQE and absorption.

$$\mathrm{EQE} = \varphi_A \times \mathrm{IQE} = \varphi_A \times \varphi_{ET1} \times \varphi_{ET2} \times (1 - \varphi_{BT}) \times \varphi_{TTA} \times \varphi_{PL} \quad (2)$$

To probe the source of improvements in EQE and IQE, we performed time-resolved upconversion photoluminescence (TRUCPL) and UC threshold measurements. We performed these measurements on 5 mg mL^{-1} PbS films with and without 3 mM TCA. To probe the effect of increasing PbS film thicknesses, we also performed these measurements on 10, 25, and 50 mg mL^{-1} PbS films with 3 mM TCA. We note that the control films (without TCA) for thicker PbS films lacked sufficient UC signal to perform TRUCPL and threshold measurements.

© 2025 Wiley-VCH GmbH

21951071, 0, Downloaded from https://advanced.onlinelibrary.wiley.com/doi/10.1002/adom.202500252 by Massachusetts Institute of Technolo, Wiley Online Library on [03/06/2025]. See the Terms and Conditions (https://onlinelibrary.wiley.com/terms-and-conditions) on Wiley Online Library for rules of use; OA articles are governed by the applicable Creative Commons License

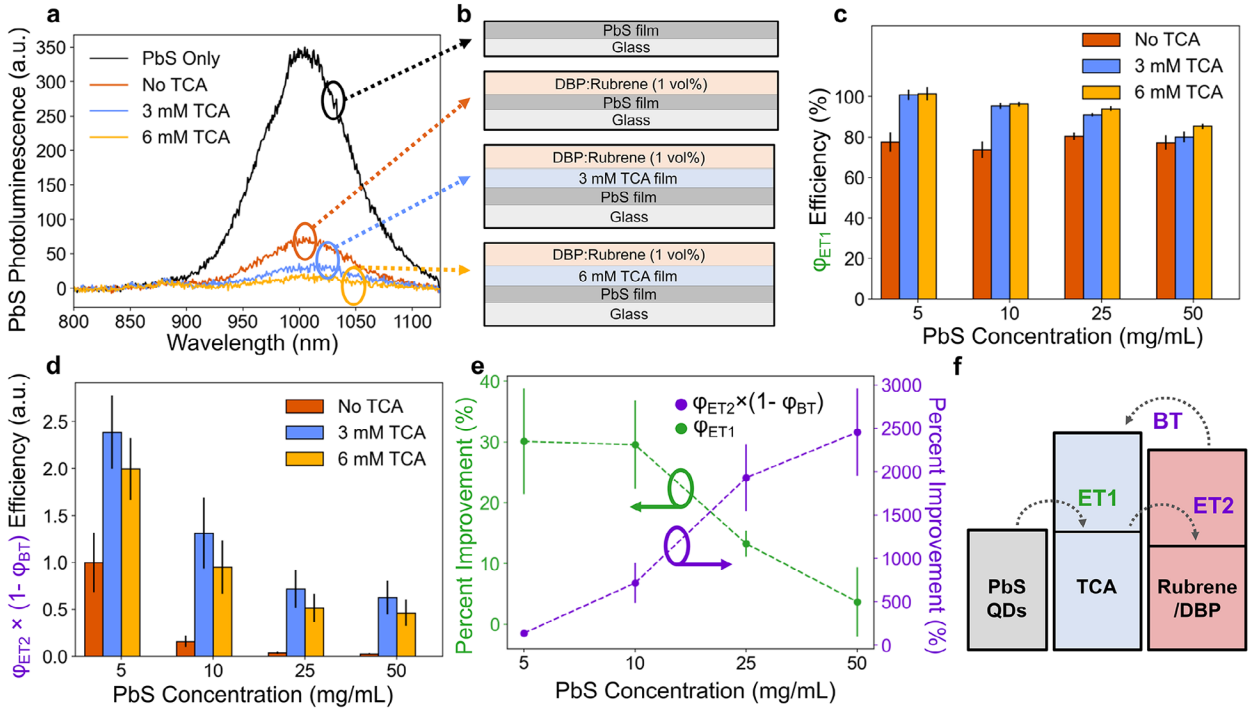

Figure 3. a) Emission spectra of different film stacks to calculate PbS QD quenching efficiencies (φ_{ET1}). b) Schematics of the film stacks fabricated. c) Efficiency of [φ_{ET1}] and d) relative efficiency of [$\varphi_{ET2} \times (1 - \varphi_{BT})$] as functions of TCA and PbS concentrations. e) Percent improvement of [φ_{ET1}] and [$\varphi_{ET2} \times (1 - \varphi_{BT})$] of 3 mM TCA films (with respect to non-TCA films) as a function of PbS concentration. f) Schematic highlighting the key energy transfer steps ET1, ET2, and BT.

The TRUCPL decays were fitted using the biexponential function in Equation (3) (see Figure 2d, Figure S11, and Table S2, Supporting Information). We observed a decrease in the average lifetime of the UC thin films with 3 mM TCA (9.11 µs) compared to control films without TCA (15.5 µs). The lifetime of UC PL decay is primarily determined by the slowest steps of UC – energy transfer from sensitizer to annihilator and the TTA process itself. Therefore, we attribute the reduced lifetime of UC PL decay upon TCA incorporation to a combination of improvements in Dexter transfer from PbS to rubrene (via TCA) and an increase in the rate of TTA due to a higher concentration of triplets in the rubrene layer.[85] Additionally, we observed a ≈50% decrease in the UC threshold for UC films with TCA (decreasing from 4.50 to 2.82 W cm^{-2}) (see Figure 2c). TCA-enhanced UC films with increasing PbS thicknesses showed a consistent drop in threshold intensity going from 2.82 W cm^{-2} for 5 mg mL^{-1} PbS to ≈1 W cm^{-2} for 50 mg mL^{-1} PbS (see Figure S10, Table S1, Supporting Information).

$$y = A_1 \exp\left(\frac{-t}{\tau_1}\right) + A_2 \exp\left(\frac{-t}{\tau_2}\right) \quad (3)$$

Both TRUCPL and threshold intensity measurements signify an increased concentration of triplets in the rubrene/DBP layer upon the introduction of TCA. Since TCA possesses a carboxylic acid group that has a strong affinity to bind to the surface of PbS QDs, we hypothesize that it behaves as an extractor/mediator ligand to aid in energy transfer to the annihilator in addition to reducing back transfer.[51,70,73] Additionally, since triplet excitons in organic semiconductors are long-lived, the extraction of excitons by semiconducting ligands helps overcome the radiative and non-radiative losses that hinder the triplet transfer from PbS QDs without extractor ligands.[53,75,78] Here, we postulate that the binding of TCA to PbS QDs increases the exciton extraction efficiency (φ_{ET1}). Still, since the UC EQE improvements could originate from either improved exciton extraction efficiency or reduced BT, we undertook further investigations to better understand the full nature of the origins of the improvements.

To investigate this ligand-effect hypothesis further, we measured the extraction efficiency of excitons from PbS (i.e., φ_{ET1}). We measured this efficiency by observing the changes in PbS photoluminescence (PL) in various thin-film configurations (see **Figure** 3b). To start, we measured the PL of PbS-only films (black curve in Figure 3a) upon 808 nm excitation. Under the same excitation intensity, we measured the PL of PbS films with 1) rubrene/DBP evaporated on top (orange curve), 2) 3 mM TCA and rubrene/DBP (blue curve), and 3) 6 mM TCA and rubrene/DBP (yellow curve). By integrating the PbS emission curve and using Equation (4), we calculated the quenching efficiency of these different configurations.

$$\varphi_{ET1} = 100 \times \frac{(\text{neat PbS film emission} - \text{UC film PbS emission})}{\text{Neat PbS film emission}} \quad (4)$$

We note that our measurement of φ_{ET1} is an approximation, as there are changes to the optical outcoupling and non-radiative pathways that are introduced when the organic layers are deposited onto the PbS film. One such non-radiative pathway would

© 2025 Wiley-VCH GmbH

21951071, 0, Downloaded from https://advanced.onlinelibrary.wiley.com/doi/10.1002/adom.202500252 by Massachusetts Institute of Technolo, Wiley Online Library on [03/06/2025]. See the Terms and Conditions (https://onlinelibrary.wiley.com/terms-and-conditions) on Wiley Online Library for rules of use; OA articles are governed by the applicable Creative Commons License

be recombination via the surface traps introduced upon the QD ligand exchange with TCA. To prove that the TCA layer deposition does not result in surface traps, we employed 9-ACA (9-anthracene carboxylic acid) as an alternative ligand which retains the carboxylic acid binding group but has a higher bandgap. The first triplet energy level of 9-ACA (≈1.83 eV) is far higher than that of TCA (≈1.3 eV) and higher than the bandgap of PbS used in this work (≈1.2 eV). Therefore, energy transfer from PbS to 9-ACA is unlikely to occur. By depositing 9-ACA (instead of TCA) on the PbS, we can probe the introduction of surface traps. As shown in Figure S12 (Supporting Information), we observe an increase in PbS PL upon spin coating comparable concentrations of 9-ACA on top of the PbS film, suggesting passivation of traps. In contrast, we observed the PbS PL to quench upon spin coating TCA (see Figure 3c), which we conclude to be resulting from exciton extraction by TCA, not via surface traps.

We observed an increase in quenching efficiency with increasing TCA concentrations (see Figure 3c). For all concentrations of PbS, without the introduction of TCA, less than 80% of the PbS emission is quenched (orange bars in Figure 3c). In stark contrast, the PbS emission from 5 and 10 mg mL^{-1} PbS films are almost completely quenched when 3 or 6 mM TCA is introduced as an interlayer between PbS and rubrene (blue and yellow bars in Figure 3c). In particular, we note that for 50 mg mL^{-1} PbS films, the quenching efficiency rises from ≈75% to over 85% upon the introduction of 6 mM TCA. This increased quenching efficiency with the introduction of TCA provides evidence of an increase in the Dexter energy transfer efficiency (φ_{ET1}) from PbS to the organic layers.

Although there is an improvement in Dexter energy transfer efficiency from QDs upon the introduction of the TCA layer, this improvement accounts for only a small fraction of the improvement in EQE. Using Equation (2), we calculated the percent improvement in the remaining $\varphi_{ET2} \times (1 - \varphi_{BT})$ term which includes the improvements resulting from back transfer alleviation (see Figure 3d). For the back transfer alleviation calculation, we used our measured values for EQE, φ_{ET1}, and DBP/rubrene PLQY (≈38%), and we assumed the φ_{TTA} to be 31% based on measurements from Di, et al.[45,51,86] Under the assumption of minimal changes in φ_{TTA}, we found that there are massive improvements in the $\varphi_{ET2} \times (1 - \varphi_{BT})$ term, especially at thicker PbS QD films (see Figure 3d). For all thicknesses of PbS films, we observe a significant increase in the $\varphi_{ET2} \times (1 - \varphi_{BT})$ term upon the introduction of 3 mM TCA. With increasing PbS film thickness, the decline in $\varphi_{ET2} \times (1 - \varphi_{BT})$ is substantial for samples without TCA (orange bars), while the decline is significantly mitigated for 3 and 6 mM TCA samples (blue and yellow bars in Figure 3d). This is likely due to the spatial separation of the donor (rubrene/DBP) and acceptor (PbS QDs) in the FRET-based energy transfer using 3 mM (≈10 nm thickness) and 6 mM TCA (≈18 nm thickness).

We note that there may be other causes for the improvement of UC performance beyond the alleviation of energy back transfer. In particular, we highlight possible changes in φ_{TTA} upon the introduction of TCA as an interlayer due to changes in rubrene crystallization.[87,88] Unfortunately, directly probing energy back transfer using fluorescence quantum yield measurements and fluorescence lifetime measurements is non-trivial in this UC system due to the highly convolved absorption spectra of PbS, TCA, rubrene, and DBP.

Figure 3e summarizes these results by plotting the percent improvement in the $\varphi_{ET2} \times (1 - \varphi_{BT})$ term and the φ_{ET1} term for different PbS concentrations. The contributions from triplet extraction decrease with an increase in PbS thickness. Meanwhile, the improvements in the $\varphi_{ET2} \times (1 - \varphi_{BT})$ term increase sharply with PbS concentration. There is a ≈(2500 ± 500)% improvement in the $\varphi_{ET2} \times (1 - \varphi_{BT})$ term while there is a (4 ± 2)% improvement in the φ_{ET1} term for 50 mg mL^{-1} PbS films. This suggests that the issues of energy back transfer to PbS QDs are far more severe for thicker PbS films, resulting in larger improvements in EQE upon the introduction of TCA as a blocker layer. By successfully addressing the bottleneck of energy back transfer while maintaining forward energy transfer, we are able to achieve manyfold higher IQEs for strongly absorbing UC films.

Given the achieved EQE improvements, we explored applications to demonstrate the practical use of this new thin-film architecture. Due to the contrasting UC performance between samples with and without TCA upon NIR excitation and the potential to pattern the TCA layer, anti-counterfeiting was particularly attractive to us. We found that the thermal deposition of TCA (≈12 nm) shows the same improvements as we observed via solution processing. We patterned the TCA layer using a shadow mask (see **Figure** 4a) followed by rubrene/DBP evaporation on the entire substrate (i.e., without a mask). Upon NIR excitation, we observed a strong contrast between TCA- and non-TCA-patterned areas.

As shown in Figure 4, we developed a simple, configurable method to uniformly pattern images for personalized anti-counterfeiting. We fabricated UC films with the Stanford University logo, the Stanford Bunny, the outline of the Stanford Memorial Church, and a simplified Congreve Lab logo upon excitation with an 850 nm LED. We captured clear pictures of the upconverted images under room lighting (see Figure S13, Supporting Information) with low excitation intensities between 10 and 100 mW cm^{-2}.

To conclude, we alleviated three issues plaguing the conventional NIR-to-visible upconverting PbS-rubrene/DBP UC films: 1) low absorption of NIR photons, 2) low energy transfer rates from PbS to rubrene/DBP, and 3) highly parasitic back transfer (BT) from rubrene/DBP to PbS. Upon incorporation of 5-tetracene carboxylic acid as a ligand and singlet-blocking layer, we achieved a champion UC EQE of 0.011% with average peak EQEs of (0.010 ± 0.001)% at 5.3 W cm^{-2} of 808 nm excitation. We uncovered the mechanism of EQE improvement, finding the back-transfer alleviation to be the primary source, especially for thicker PbS films. Additionally, the EQE improvement in this NIR-to-visible regime is a key step toward the realization of TTA-UC in photovoltaics, night vision, and anti-counterfeiting technologies. We believe this work functions as a proof of concept of a thin-film UC architecture which can be broadened to other solid-state systems to improve efficiencies for practical incorporation in real-world applications.

3. Experimental Section

Materials: Rubrene (>99%, purified by sublimation) was purchased from TCI America. 5-tetracene carboxylic acid (>95% by NMR) was

© 2025 Wiley-VCH GmbH

21951071, 0, Downloaded from https://advanced.onlinelibrary.wiley.com/doi/10.1002/adom.202500252 by Massachusetts Institute of Technolo, Wiley Online Library on [03/06/2025]. See the Terms and Conditions (https://onlinelibrary.wiley.com/terms-and-conditions) on Wiley Online Library for rules of use; OA articles are governed by the applicable Creative Commons License

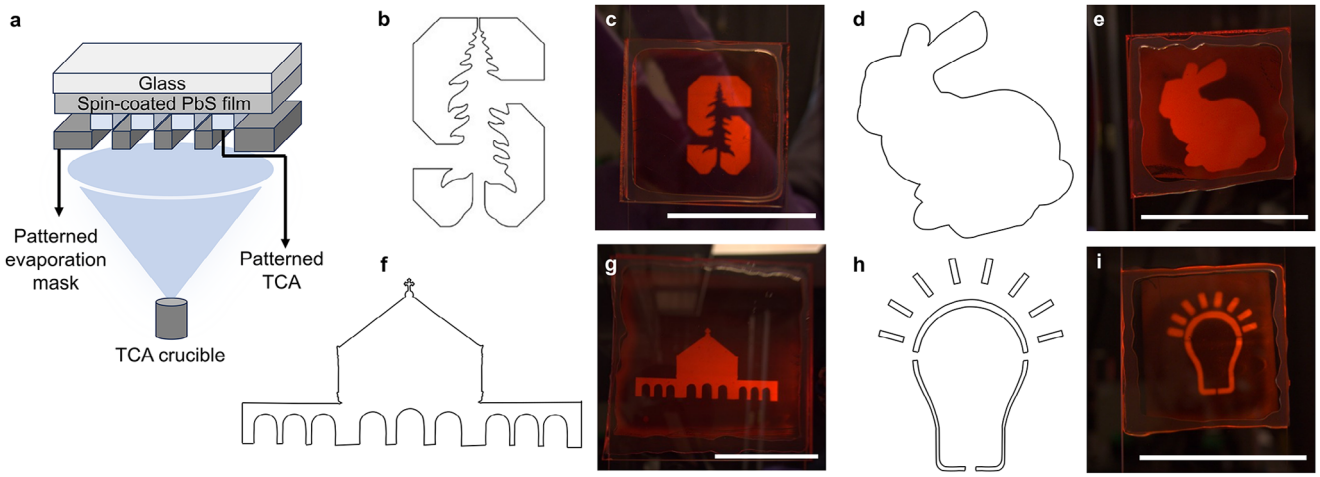

Figure 4. a) Schematic illustration of patterning of TCA layer via thermal deposition. Images for evaporation mask laser cutting: b) Stanford logo, d) Stanford Bunny, f) Stanford Memorial Church outline, h) Congreve Lab logo outline. Unedited images of upconversion under 850 nm LED illumination with 200 millisecond exposure time: c) Stanford logo, e) Stanford Bunny, g) Memorial Church outline, i) Bulb outline from Congreve Lab logo. The scale bar is 1 inch in length.

purchased from HAARES ChemTech Inc. PbO (Puratronic, 99.999%, metals basis), 1-octadecene (90%, technical grade), anhydrous toluene (99.85%, extra dry over molecular sieves, AcroSeal), and anhydrous acetonitrile (99.9+%, extra dry, AcroSeal) were purchased from Thermo Scientific Chemicals. Oleic acid (technical grade, 90%), DBP (5,10,15,20-Tetraphenylbisbenz[5,6]indeno[1,2,3-cd:1′,2′,3′-lm]perylene, 98% HPLC), and hexamethyldisilathiane (synthesis grade) were purchased from Millipore Sigma. Hexanes (certified ACS), isopropanol (ACS-certified), and acetone (ACS-certified) were purchased from Fisher Scientific. All chemicals were used as purchased unless specified.

Synthesis of PbS Quantum Dots (930 nm Absorption Peak): PbS quantum dots were fabricated using a modified Hines hot-injection technique.[89] To a two-neck 100 mL round bottom flask, 0.669 g of PbO, 30 mL of 1-octadecene, and 2 mL of oleic acid were added. The flask was heated under vacuum to degas and synthesize lead oleate (temperature was increased to 120 °C slowly at 10 °C every 10 min). The reaction flask was degassed at 120 °C for at least 4 h resulting in a clear solution. The injection temperature was set to 105 °C and the flask was refilled with nitrogen. In a nitrogen atmosphere glovebox, 7.5 mL of dry toluene was charged with 350 µL of hexamethyldisilathiane. This solution was removed from the glovebox (<0.1 ppm O_2, <0.5 ppm H_2O) and injected into the reaction flask with minimal exposure to air. Upon injection, the reaction flask was immediately removed from the hot plate and allowed to air cool. Upon reaching room temperature, the reaction was washed with acetone (4× volume of acetone was added and centrifuged at 8800 × g for 2 mins). The resulting pellet was redispersed in hexanes (≈30 mL) and washed with acetone (×4 volume of acetone was added and centrifuged at 8800 × g for 2 mins). The final pellet was redispersed in hexanes (≈15 mL) and stored in the glovebox until use.

TCA Triplet Energy: The triplet energy of TCA was reported by Luo, et al. to be ≈1.3 eV, which was an approximation based on the measured triplet energy level of tetracene, a close chemical analog of TCA.[83]

Fabrication of Upconversion Films–Substrate Treatment: All samples, unless otherwise specified, were fabricated on 1 cm × 1 cm soda-lime glass of thickness 1.1 mm. All substrates were washed by sonicating for 10 min in a 1% Hellmanex detergent solution in deionized water, followed by two 5-minutes sonications in deionized water, followed by two 5-minute sonications in acetone, and two 5-minute sonications in isopropanol. The substrates were then dried under pressurized air to remove solvent and dust particles. Within 15 min before spin coating, the glass substrates were treated with UV ozone plasma for at least 15 min.

Solution Preparation: The PbS QDs stock solution was washed with acetone once more (4× acetone, 8800 rcf for 2 mins) to create a pellet. In a nitrogen-filled glovebox, this weighed pellet was dissolved in anhydrous toluene to make the solutions with the desired concentrations (5, 10, 25, and 50 mg mL^{-1} via serial dilution) and filtered through 0.2 µm PTFE membrane syringe filters (Titan3, 17 mm, filter blue) before spin coating. In a nitrogen-filled glovebox, a 10 mM stock solution of TCA in anhydrous acetonitrile was prepared by heating the solution at ≈70 °C overnight. After cooling, the resulting solution was filtered through Titan3, 17 mm, filter blue 0.2 µm PTFE membrane syringe filters and diluted as needed (3 or 6 mM TCA in acetonitrile) before spin coating.

Spin Coating: All spin coating was performed in a nitrogen-filled glovebox. PbS QD solutions in toluene (80 µL) were spin-coated at 1500 rpm for 30 s with a 0.8 s ramp (1875 rpm s^{-1} ramp). TCA solutions in acetonitrile (100 µL) were spun on top of the PbS QD film with the same spin conditions. After the spin(s), the substrates were annealed on a hot plate at 70 °C for 15 min.

Thermal Evaporation: The spin-coated substrates were then loaded into an Angstrom Engineering thermal evaporation chamber. All evaporations were performed under a pressure of less than 1E-05 mbar. DBP-doped (1% v/v) rubrene evaporations were performed by co-evaporating the chemicals from two different sources. For 1% doping, the DBP was evaporated at a rate of ≈0.02–0.03 Å s^{-1} while the rubrene was evaporated at ≈2–3 Å s^{-1}. Both DBP and rubrene were evaporated from resistively heated alumina crucibles. The rubrene/DBP films had a final thickness of ≈64 nm based on profilometry. This rubrene thickness showed the best performance for these UC films.

Encapsulation: All samples were encapsulated with a 1.2 mm-thick microscope slide (Electron Microscopy Sciences) using Norland Optical NOA81 (Thorlabs) fast-curing optical adhesive cured under a UV lamp for 2 min.

Photoluminescence Quantum Yield (PLQY) Measurement: Photoluminescence quantum yields of rubrene/DBP films were measured using the de Mello method in an integrating sphere (from Labsphere).[90] The integrating sphere was calibrated using a radiometric light source (HL-3P-INT-CAL, Ocean Insight). A 447 nm continuous wave laser was used to excite the neat rubrene/DBP (≈64 nm) films. The sample was loaded into the sphere such that the 447 m laser had an ≈8° incidence.

Steady-State Photoluminescence and UC Photoluminescence Measurement: All relative PL and UCPL measurements were conducted on the set up shown in Figure S6 (Supporting Information). The samples were illuminated with an 808 nm continuous wave laser at an angle

© 2025 Wiley-VCH GmbH

21951071, 0, Downloaded from https://advanced.onlinelibrary.wiley.com/doi/10.1002/adom.202500252 by Massachusetts Institute of Technolo, Wiley Online Library on [03/06/2025]. See the Terms and Conditions (https://onlinelibrary.wiley.com/terms-and-conditions) on Wiley Online Library for rules of use; OA articles are governed by the applicable Creative Commons License

of ≈45 degrees. The emission from the samples was collected using a high NA lens and fiber-coupled spectrometer (QE pro high-performance, Ocean Insight). The fiber coupling to the detector included a filter holder. A 750 nm short pass filter (Thorlabs) was used to filter the laser out of the UCPL spectra. An 850 nm long pass filter (Thorlabs) was used to filter the laser out of the PbS QD PL spectra.

To calculate upconversion photoluminescence, the emission was integrated from 500–700 nm. To calculate the PbS photoluminescence, the emission was integrated from 900–1100 nm. Integration times and scans to average were adjusted to achieve high signal-to-noise ratios.

Upconversion External Quantum Efficiency Measurement: It is found that a traditional integrating sphere method for EQE measurement suffered from 1) signal-to-noise constraints, 2) laser signal saturation, and 3) UC emission reabsorption, which were non-trivial to account for. The photoluminescence set up described above was used for the EQE measurements. Therefore, to measure the EQEs, the method introduced by Izawa et al. was used.[45] A rubrene/DBP-only film (≈64 nm) was used as the standard with a known PLQY. This standard was used because its fabrication process and form factor most closely resemble the UC film itself; the only difference being that the standard film lacks the PbS QDs and TCA which were incorporated in UC films. The PLQY of this standard was ≈38%. This PLQY measurement was done using a 447 nm laser via the De Mello methodology described above.

The PL (integrated 500–700 nm) from rubrene/DBP-only samples (I_{std}) was measured using a 447 nm continuous wave laser. With the same optical alignment, the UCPL (integrated 500–700 nm) from upconversion films (I_{UC}) was measured using an 808 nm continuous wave laser with an intensity of 5.3 W cm^{-2}. The incident power of the 447 nm (P_{std}) and 808 nm (P_{UC}) lasers was measured using a Thorlabs power meter (PM100D meter with S120VC sensor). All measurements were performed with a 750 nm short pass filter (Thorlabs). For each UC film stack, triplicates were fabricated and 4 points on each sample were measured with random positions. The resulting averages and standard deviations were propagated using the Python uncertainties package. Equation (5) was used to calculate the EQEs of the different films.

$$\mathrm{EQE} = \frac{I_{UC}}{I_{Std}} \times \frac{P_{Std}}{P_{UC}} \times (\%A_{Std}) \times \mathrm{PLQY}_{Std} \quad (5)$$

PbS Photoluminescence Quenching Measurement: The photoluminescence setup was used with an 850 nm long pass filter (Thorlabs) to perform measurements of PbS PL (integrated from 900–1100 nm). The UC films were excited using an 808 nm laser at 0.56 W cm^{-2} intensity. Each thin-film stack was prepared in triplicates and 4 measurements were performed on each substrate randomly. The resulting averages and standard deviations were propagated using the Python uncertainties package. Quenching efficiencies were calculated using Equation (4). PbS-only films were used to calculate PL_{PbS}, while PbS-rubrene/DBP and PbS-TCA-rubrene/DBP films were used to calculate PL_{UC}.

Upconversion Threshold Measurement: The upconversion threshold was measured using the photoluminescence set up described above. The laser was set to the highest power required for the measurement and the power was attenuated using ND filters. The UC PL for the samples was measured across orders of magnitude of input power to span the linear and quadratic regimes in the log–log input-output power plots. The integration times were increased to achieve high signals at low input powers.

The input power for each point was measured using a Thorlabs power meter (PM100D meter with S120VC sensor). The spot-size of the input laser was measured using a camera to calculate the intensity of the input light. The threshold intensity was calculated by fitting the log–log plot in the linear and quadratic regimes to find the abscissa of the point of intersection of those lines.

Note: The upconversion threshold was measured for 5 mg mL^{-1} PbS with and without 3 mM TCA. This was because, with thicker PbS (25 and 50 mg mL^{-1}), there were insufficient UC signals from the control (no TCA) samples to measure the threshold. The same samples (5 mg mL^{-1} with and without 3 mM TCA) were used to measure the TRUCPL.

Spot-size measurement: Spot-sizes were calculated using a Zelux 1.6 MP Color CMOS camera. ND filters were used to prevent saturation of the camera. The full width at half maximum was calculated. Since the measurements were performed at 45° incidence, an ellipsoidal area was calculated from the spot-size.

Time-Resolved Upconversion Photoluminescence Spectroscopy Measurement: The TRUCPL decays were collected using a Streakscope C10627 from Hamamatsu Corp. A Dragon Laser H Series 808 nm was pulsed by a function generator RIGOL DG812.

UV–Vis Spectroscopy (Absorption) Measurement: UV–vis spectroscopy was performed on 50 mg mL^{-1} PbS films (encapsulated) using an Agilent Cary 6000i UV/vis/NIR machine in transmission mode. For solution-state measurements, a 1 cm path-length quartz cuvette was used. The PbS QDs solution-state absorption was measured in hexanes with a baseline of the absorption of hexanes neat. A second relative method was also used to calculate the absorption values, which resulted in similar values (see SI for more information).

Atomic Force Microscopy Measurement: The AFM images were taken in ambient air by NX-10 in non-contact mode. The film (5 mg mL^{-1} with 6 mM TCA) was cut using a blade to measure the thickness.

Profilometry Measurement: A Dektak XT-S Stylus profilometer was used under 3 mg stylus force, with grooves scratched into the samples with a razor blade for measurement.

Fabrication of Evaporation Masks: Evaporation masks were fabricated through laser cutting of aluminum metal sheets using FabLight FL4500.

Fabrication of Anti-Counterfeiting UC Films: This fabrication was performed on 1 inch × 1 inch or 2 inch × 2 inch (for the Stanford Memorial Church image) soda-lime glass substrates. These substrates were washed and treated as described above. While spin coating, 350 µL of 10 mg mL^{-1} PbS QD solution was used. Instead of spin coating TCA in acetonitrile, neat TCA was thermally evaporated onto the PbS QD film through a shadow mask at a rate of 1–3 Å s^{-1} from a resistively heated crucible. The rubrene/DBP was then evaporated onto the entire substrate without a mask. The thin films were encapsulated using EpoTek UV-curing epoxy glue.

Imaging of Anti-Counterfeiting UC Thin Films: An 850 nm LED from Thorlabs (M850L3) was used as the excitation source. A camera (Kiralux 8.9 MP Color CMOS Camera) was mounted with an imaging lens to take pictures of the substrates. Images were taken under 200 ms exposure time. See Figure S13 (Supporting Information). Excitation power was measured using a power meter (PM100D meter with S120VC sensor). NOTE: the image of Memorial Church was taken under waveguided excitation due to the large size (2 inch × 2 inch) of the substrate.

Supporting Information

Supporting Information is available from the Wiley Online Library or from the author.

Acknowledgements

Part of this work was performed at the Stanford Nano Shared Facilities (SNSF), supported by the National Science Foundation under award ECCS-2026822. Part of this work was performed at Lab64, the EE Makerspace at Stanford University. The authors would like to acknowledge the Stanford Computer Graphics Laboratory for the Stanford Bunny image. P.N. acknowledges the support of a Stanford Graduate Fellowship in Science & Engineering (SGF) as a Gabilan Fellow and the Chevron Fellowship in Energy. M.H. acknowledges the support of the Department of Electrical Engineering at Stanford University. A.O.G. acknowledges the support of a National Science Foundation Graduate Research Fellowship under grant DGE-1656518 and a Stanford Graduate Fellowship in Science & Engineering (SGF) as a Scott A. and Geraldine D. Macomber Fellow. L.P. acknowledges the support of a National Science Foundation Graduate Research Fellowship under grant DGE-2146755. T.H.S. acknowledges the support of the Arnold O. Beckman Postdoctoral Fellowship. S.F. acknowledges the

© 2025 Wiley-VCH GmbH

21951071, 0, Downloaded from https://advanced.onlinelibrary.wiley.com/doi/10.1002/adom.202500252 by Massachusetts Institute of Technolo, Wiley Online Library on [03/06/2025]. See the Terms and Conditions (https://onlinelibrary.wiley.com/terms-and-conditions) on Wiley Online Library for rules of use; OA articles are governed by the applicable Creative Commons License

support from Stanford University as a Diversifying Academia, Recruiting Excellence (DARE) Fellow, the U.S. Department of Energy (DOE) Building Technologies Office (BTO) as an IBUILD Graduate Research Fellow, Stanford Graduate Fellowship in Science & Engineering (SGF) as a P. Michael Farmwald Fellow, and of the National GEM Consortium as a GEM Fellow. K.M.K.Y. acknowledges the Chevron Energy Fellowship and the Stanford DARE fellowship for partial support. W.M. and N.M. acknowledge support from the Stanford University Department of Electrical Engineering through the Research Experience for Undergraduates (REU) program. V.M. acknowledges support from the Stanford University School of Engineering through the Stanford Undergraduate Research Fellowship (SURF) program. R.H. acknowledges the support of the Chancellor's Opportunity Fellowship. This research was performed under an appointment to the Building Technologies Office (BTO) IBUILD Graduate Research Fellowship administered by the Oak Ridge Institute for Science and Education (ORISE) and managed by Oak Ridge National Laboratory (ORNL) for the DOE. ORISE is managed by Oak Ridge Associated Universities (ORAU). All opinions expressed in this paper are the authors' and do not necessarily reflect the policies and views of the DOE, EERE, BTO, ORISE, ORAU, or ORNL. Funding SourcesFunding from the Defense Advanced Research Projects Agency grant HR00112220010 (PN, MH, EB, LP, GA, DF, RH, MK, DC) is acknowledged. T.F.J. and K.M.K.Y. acknowledge support from the Liquid Sunlight Alliance, which is supported by the U.S. Department of Energy, Office of Science, Office of Basic Energy Sciences, Fuels from Sunlight Hub under Award Number DE-SC0021266 for template design for system demonstration.

Conflict of Interest

DNC is a co-founder of and Chief Scientific Advisor to Quadratic 3D, Inc.

Author Contributions

Conceptualization was done by P.N., M.H., G.A., E.B., and D.N.C. Methodology was done by P.N., M.H., A.O.G., and Q.Z. Investigation and interpretation was done by P.N., M.H., A.O.G., L.P., Q.Z., E.B., G.A., S.F., W.M., N.M., V.M., D.F., R.H., T.H.S., and K.M.K.Y. Supervision was done by T.F.J., M.A.K., and D.N.C. The original draft was written by P.N. All authors dealt with writing review and editing. Funding acquisition was done by M.A.K. and D.N.C.

Data Availability Statement

The data that support the findings of this study are available from the corresponding author upon reasonable request;

Keywords

anti-counterfeiting, near infrared, PbS quantum dots, tetracene-5-carboxylic acid, triplet–triplet annihilation, upconversion

Received: January 23, 2025
Revised: April 11, 2025
Published online:

[1] A. J. Carrod, V. Gray, K. Börjesson, *Energy Environ. Sci.* **2022**, *15*, 4982.
[2] T. F. Schulze, J. Czolk, Y. Y. Cheng, B. Fückel, R. W. MacQueen, T. Khoury, M. J. Crossley, B. Stannowski, K. Lips, U. Lemmer, A. Colsmann, T. W. Schmidt, *J. Phys. Chem. C* **2012**, *116*, 22794.
[3] J. C. Goldschmidt, S. Fischer, J. C. Goldschmidt, S. Fischer, *Adv. Opt. Mater.* **2015**, *3*, 510.
[4] R. Singh, E. Madirov, D. Busko, I. M. Hossain, V. A. Konyushkin, A. N. Nakladov, S. V. Kuznetsov, A. Farooq, S. Gharibzadeh, U. W. Paetzold, B. S. Richards, A. Turshatov, *ACS Appl. Mater. Interfaces* **2021**, *13*, 54874.
[5] M. Kinoshita, Y. Sasaki, S. Amemori, N. Harada, Z. Hu, Z. Liu, L. K. Ono, Y. Qi, N. Yanai, N. Kimizuka, *ChemPhotoChem* **2020**, *4*, 5271.
[6] S.-W. Liu, C.-C. Lee, C.-H. Yuan, W.-C. Su, S.-Y. Lin, W.-C. Chang, B.-Y. Huang, C.-F. Lin, Y.-Z. Lee, T.-H. Su, K.-T. Chen, S.-W. Liu, C.-F. Lin, Y.-Z. Lee, T.-H. Su, C.-C. Lee, C.-H. Yuan, W.-C. Su, S.-Y. Lin, W.-C. Chang, B.-Y. Huang, K.-T. Chen, *Adv. Mater.* **2015**, *27*, 1217.
[7] R. Hamid, D. Feng, P. Narayanan, J. S. Edwards, M. Hu, E. Belliveau, M. Kim, S. Deshpande, C. Wan, L. Pucurimay, D. A. Czaplewski, D. N. Congreve, M. A. Kats, *arXiv:2411.18707* **2024**.
[8] B. D. Ravetz, A. B. Pun, E. M. Churchill, D. N. Congreve, T. Rovis, L. M. Campos, *Nature* **2019**, *565*, 343.
[9] B. Pfund, D. M. Steffen, M. R. Schreier, M. S. Bertrams, C. Ye, K. Börjesson, O. S. Wenger, C. Kerzig, *J. Am. Chem. Soc.* **2020**, *142*, 10468.
[10] L. Huang, W. Wu, Y. Li, K. Huang, L. Zeng, W. Lin, G. Han, *J. Am. Chem. Soc.* **2020**, *142*, 18460.
[11] A. L. Hagstrom, S. Weon, W. Choi, J. H. Kim, *ACS Appl. Mater. Interfaces* **2019**, *11*, 13304.
[12] S. H. C. Askes, S. Bonnet, *Nat. Rev. Chem.* **2018**, *2*, 437.
[13] O. S. Kwon, H. S. Song, J. Conde, H. I.l Kim, N. Artzi, J. H. Kim, *ACS Nano* **2016**, *10*, 1512.
[14] S. Mattiello, A. Monguzzi, J. Pedrini, M. Sassi, C. Villa, Y. Torrente, R. Marotta, F. Meinardi, L. Beverina, *Adv. Funct. Mater.* **2016**, *26*, 8447.
[15] C. Wohnhaas, A. Turshatov, V. Mailänder, S. Lorenz, S. Baluschev, T. Miteva, K. Landfester, *Macromol. Biosci.* **2011**, *11*, 772.
[16] Q. Liu, T. Yang, W. Feng, F. Li, *J. Am. Chem. Soc.* **2012**, *134*, 5390.
[17] Q. Liu, B. Yin, T. Yang, Y. Yang, Z. Shen, P. Yao, F. Li, *J. Am. Chem. Soc.* **2013**, *135*, 5029.
[18] Q. Liu, M. Xu, T. Yang, B. Tian, X. Zhang, F. Li, *ACS Appl. Mater. Interfaces* **2018**, *10*, 9883.
[19] M. You, J. Zhong, Y. Hong, Z. Duan, M. Lin, F. Xu, *Nanoscale* **2015**, *7*, 4423.
[20] W. Yin, T. Yu, J. Chen, R. Hu, G. Yang, Y. Zeng, Y. Li, *ACS Appl. Mater. Interfaces* **2021**, *13*, 57481.
[21] H. Suo, Q. Zhu, X. Zhang, B. Chen, J. Chen, F. Wang, *Mater. Today Phys.* **2021**, *21*, 100520.
[22] S. N. Sanders, T. H. Schloemer, M. K. Gangishetty, D. Anderson, M. Seitz, A. O. Gallegos, R. C. Stokes, D. N. Congreve, *Nature* **2022**, *604*, 474.
[23] D. K. Limberg, J. H. Kang, R. C. Hayward, *J. Am. Chem. Soc.* **2022**, *144*, 5226.
[24] C. J. O'dea, J. Isokuortti, E. E. Comer, S. T. Roberts, Z. A. Page, *Polym. Sci.* **2023**, *195*, 112193
[25] J. Wong, S. Wei, R. Meir, N. Sadaba, N. A. Ballinger, E. K. Harmon, X. Gao, G. Altin-Yavuzarslan, L. D. Pozzo, L. M. Campos, A. Nelson, J. Wong, N. Sadaba, N. A. Ballinger, G. Altin-Yavuzarslan, A. Nelson, S. Wei, R. Meir, X. Gao, L. M. Campos, E. K. Harmon, L. D. Pozzo, *Adv. Mater.* **2023**, *35*, 2207673.
[26] T. Schloemer, P. Narayanan, Q. Zhou, E. Belliveau, M. Seitz, D. N. Congreve, *ACS Nano* **2023**, *17*, 3259.
[27] M. P. Rauch, R. R. Knowles, *Chimia* **2018**, *72*, 501.
[28] J. Zhou, Q. Liu, W. Feng, Y. Sun, F. Li, *Chem. Rev.* **2015**, *115*, 395.
[29] S. E. Seo, H. S. Choe, H. Cho, H. I.l Kim, J. H. Kim, O. S. Kwon, *J. Mater. Chem. C Mater.* **2022**, *10*, 4483.
[30] Y. Ji, W. Xu, N. Ding, H. Yang, H. Song, Q. Liu, H. Ågren, J. Widengren, H. Liu, *Light: Sci. Appl.* **2020**, *9*, 184.
[31] G. Liang, H. Wang, H. Shi, H. Wang, M. Zhu, A. Jing, J. Li, G. Li, *J. Nanobiotechnol.* **2020**, *18*, 1.
[32] S. Borse, R. Rafique, Z. V. P. Murthy, T. J. Park, S. K. Kailasa, *Analyst* **2022**, *147*, 3155.

 © 2025 Wiley-VCH GmbH

21951071, 0, Downloaded from https://advanced.onlinelibrary.wiley.com/doi/10.1002/adom.202500252 by Massachusetts Institute of Technolo, Wiley Online Library on [03/06/2025]. See the Terms and Conditions (https://onlinelibrary.wiley.com/terms-and-conditions) on Wiley Online Library for rules of use; OA articles are governed by the applicable Creative Commons License

[33] C. Duan, L. Liang, L. Li, R. Zhang, Z. P. Xu, *J. Mater. Chem. B* **2018**, *6*, 192.
[34] Upconversion Nanomaterials in, T. Bioimaging, B. Applications, Z. Gerelkhuu, Y.-I. Lee, T. Hyun Yoon, *Nanomaterials* **2022**, *12*, 3470.
[35] F. Auzel, *Chem. Rev.* **2004**, *104*, 139.
[36] C. Lee, E. Z. Xu, Y. Liu, A. Teitelboim, K. Yao, A. Fernandez-Bravo, A. M. Kotulska, S. H. Nam, Y. D. Suh, A. Bednarkiewicz, B. E. Cohen, E. M. Chan, P. J. Schuck, *Nature* **2021**, *589*, 230.
[37] D. H. Weingarten, M. D. Lacount, J. Van De Lagemaat, G. Rumbles, M. T. Lusk, S. E. Shaheen, *Nat. Commun.* **2017**, *8*, 14808.
[38] T. N. Singh-Rachford, F. N. Castellano, *Coord. Chem. Rev.* **2010**, *254*, 2560.
[39] Z. Huang, M. Lee Tang, *J. Phys. Chem. Lett.* **2018**, *9*, 6198.
[40] M. Wu, D. N. Congreve, M. W. B. Wilson, J. Jean, N. Geva, M. Welborn, T. Van Voorhis, V. Bulovic, M. G. Bawendi, M. A. Baldo, *Nat. Photonics* **2015**, *10*, 31.
[41] L. Nienhaus, M. Wu, N. Geva, J. J. Shepherd, M. W. B. Wilson, V. Bulović, T. Van Voorhis, M. A. Baldo, M. G. Bawendi, *ACS Nano* **2017**, *11*, 7848.
[42] N. Yanai, N. Kimizuka, *Acc. Chem. Res.* **2017**, *50*, 2487.
[43] T. C. Wu, D. N. Congreve, M. A. Baldo, *Appl. Phys. Lett.* **2015**, *107*, 031103.
[44] A. Monguzzi, R. Tubino, S. Hoseinkhani, M. Campione, F. L. P. Meinardi, *Phys. Chem. Chem. Phys.* **2012**, *14*, 4322.
[45] S. Izawa, M. Hiramoto, *Nat. Photonics* **2021**, *15*, 895.
[46] Y. Sakamoto, S. Izawa, H. Ohkita, M. Hiramoto, Y. Tamai, *Commun. Mater.* **2022**, *3*, 76.
[47] Y. Zhou, F. N. Castellano, T. W. Schmidt, K. Hanson, *ACS Energy Lett.* **2020**, *5*, 2322.
[48] P. Bharmoria, H. Bildirir, K. Moth-Poulsen, *Chem. Soc. Rev.* **2020**, *49*, 6529.
[49] D. G. Bossanyi, Y. Sasaki, S. Wang, D. Chekulaev, N. Kimizuka, N. Yanai, J. Clark, *J. Mater. Chem. C Mater.* **2022**, *10*, 4684.
[50] S.-J. Wang, A. Kirch, M. Sawatzki, T. Achenbach, H. Kleemann, S. Reineke, K. Leo, S.-J. Wang, A. Kirch, M. Sawatzki, T. Achenbach, H. Kleemann, S. Reineke, K. Leo, *Adv. Funct. Mater.* **2023**, *33*, 2213768.
[51] M. Hu, E. Belliveau, Y. Wu, P. Narayanan, D. Feng, R. Hamid, N. Murrietta, G. H. Ahmed, M. A. Kats, D. N. Congreve, *ACS Nano* **2023**, *17*, 22642.
[52] P. Bi, T. Zhang, Y. Guo, J. Wang, X. W. Chua, Z. Chen, W. P. Goh, C. Jiang, E. E. M. Chia, J. Hou, L. Yang, *Nat. Commun.* **2024**, *15*, 5719.
[53] M. Mahboub, Z. Huang, M. L. Tang, *Nano Lett.* **2016**, *16*, 7169.
[54] R. Weiss, Z. A. Vanorman, C. M. Sullivan, L. Nienhaus, *ACS Mater. Au* **2022**, *2*, 641.
[55] L. Nienhaus, M. Wu, V. Bulović, M. A. Baldo, M. G. Bawendi, *Dalton Trans.* **2018**, *47*, 8509.
[56] J. Duan, Y. Liu, Y. Zhang, Z. Chen, X. Xu, L. Ye, Z. Wang, Y. Yang, D. Zhang, H. Zhu, *Sci. Adv.* **2022**, *8*, 4935.
[57] R. Dziobek-Garrett, C. J. Imperiale, M. W. B. Wilson, T. J. Kempa, *Nano Lett.* **2023**, *23*, 4837.
[58] S. Baluschev, V. Yakutkin, T. Miteva, G. Wegner, T. Roberts, G. Nelles, A. Yasuda, S. Chernov, S. Aleshchenkov, A. Cheprakov, *New J. Phys.* **2008**, *10*, 013007.
[59] F. Deng, J. R. Sommer, M. Myahkostupov, K. S. Schanze, F. N. Castellano, *Chem. Commun.* **2013**, *49*, 7406.
[60] E. Radiunas, S. Raišys, S. Juršenas, A. Jozeliunaite, T. Javorskis, U. Šinkeviciute, E. Orentas, K. Kazlauskas, *J. Mater. Chem. C Mater.* **2020**, *8*, 5525.
[61] Y. Sasaki, N. Yanai, N. Kimizuka, *Inorg. Chem.* **2022**, *61*, 5982.
[62] J. Zhang, R. W. Crisp, J. Gao, D. M. Kroupa, M. C. Beard, J. M. Luther, *J. Phys. Chem. Lett.* **2015**, *6*, 1830.
[63] S. Amemori, R. K. Gupta, M. L. Böhm, J. Xiao, U. Huynh, T. Oyama, K. Kaneko, A. Rao, N. Yanai, N. Kimizuka, *Dalton Trans.* **2018**, *47*, 8590.
[64] V. Gray, D. T. W. Toolan, S. Dowland, J. R. Allardice, M. P. Weir, Z. Zhang, J. Xiao, A. Klimash, J. F. Winkel, E. K. Holland, G. M. Fregoso, J. E. Anthony, H. Bronstein, R. Friend, A. J. Ryan, R. A. L. Jones, N. C. Greenham, A. Rao, *J. Am. Chem. Soc.* **2024**, *146*, 7763.
[65] N. Tripathi, K. Kamada, *ACS Appl. Nano Mater.* **2024**, *7*, 2950.
[66] M. Wu, J. Jean, V. Bulović, M. A. Baldo, *Appl. Phys. Lett.* **2017**, *110*, 211101.
[67] M. Wu, T. A. Lin, J. O. Tiepelt, V. Bulović, M. A. Baldo, *Nano Lett.* **2021**, *21*, 1011.
[68] J. Liao, W. Guo, X. Luo, *J. Photochem. Photobiol.* **2022**, *11*, 100128.
[69] V. Gray, J. R. Allardice, Z. Zhang, S. Dowland, J. Xiao, A. J. Petty, J. E. Anthony, N. C. Greenham, A. Rao, *ACS Nano* **2020**, *14*, 4224.
[70] J. Alves, J. Feng, L. Nienhaus, T. W. C. Schmidt, *J. Mater. Chem. C Mater.* **2022**, *10*, 7783.
[71] S. Wen, J. Zhou, P. J. Schuck, Y. D. Suh, T. W. Schmidt, D. Jin, *Nat. Photonics* **2019**, *13*, 828.
[72] B. Y. Lin, C. J. Easley, C. H. Chen, P. C. Tseng, M. Z. Lee, P. H. Sher, J. K. Wang, T. L. Chiu, C. F. Lin, C. J. Bardeen, J. H. Lee, *ACS Appl. Mater. Interfaces* **2017**, *9*, 10963.
[73] N. Geva, L. Nienhaus, M. Wu, V. Bulović, M. A. Baldo, T. Van Voorhis, M. G. Bawendi, *J. Phys. Chem. Lett.* **2019**, *10*, 3147.
[74] N. Tripathi, M. Ando, T. Akai, K. Kamada, *ACS Appl. Nano Mater.* **2021**, *4*, 9680.
[75] V. Gray, W. Drake, J. R. Allardice, Z. Zhang, J. Xiao, D. G. Congrave, J. Royakkers, W. Zeng, S. Dowland, N. C. Greenham, H. Bronstein, J. E. Anthony, A. Rao, *J. Mater. Chem. C Mater.* **2022**, *10*, 16321.
[76] Z. L. Teh, L. Hu, Z. Zhang, A. R. Gentle, Z. Chen, Y. Gao, L. Yuan, Y. Hu, T. Wu, R. J. Patterson, S. Huang, *ACS Appl. Mater. Interfaces* **2020**, *12*, 22751.
[77] Z. Huang, Z. Xu, M. Mahboub, Z. Liang, P. Jaimes, P. Xia, K. R. Graham, M. L. Tang, T. Lian, *J. Am. Chem. Soc.* **2019**, *141*, 9769.
[78] Z. Huang, M. L. Tang, *J. Am. Chem. Soc.* **2017**, *139*, 9412.
[79] T.-A. Lin, C. F. Perkinson, M. A. Baldo, T. Lin, M. A. Baldo, C. F. Perkinson, *Adv. Mater.* **2020**, *32*, 1908175.
[80] C.-H. Chen, N. T. Tierce, M. Leung, T.-L. Chiu, C.-F. Lin, C. J. Bardeen, J.-H. Lee, C. Chen, J. Lee, N. T. Tierce, C. J. Bardeen, M. Leung, T. Chiu, C. Lin, *Adv. Mater.* **2018**, *30*, 1804850.
[81] Y. Deng, L. Jiang, L. Huang, T. Zhu, *ACS Energy Lett.* **2022**, *2022*, 847.
[82] A. Sawa, S. Shimada, N. Tripathi, C. Heck, H. Tachibana, E. Koyama, T. Mizokuro, Y. Hirao, T. Kubo, N. Tamai, D. Kuzuhara, H. Yamada, K. Kamada, *J. Mater. Chem. C Mater.* **2023**, *11*, 8502.
[83] A. K. Pandey, *Sci. Rep.* **2015**, *5*, 7787.
[84] X. Luo, Y. Han, Z. Chen, Y. Li, G. Liang, X. Liu, T. Ding, C. Nie, M. Wang, F. N. Castellano, K. Wu, *Nat. Commun.* **2020**, *11*, 28.
[85] A. Ronchi, A. Monguzzi, *J. Appl. Phys.* **2021**, *129* , 50901.
[86] D. Di, L. Yang, J. M. Richter, L. Meraldi, R. M. Altamimi, A. Y. Alyamani, D. Credgington, K. P. Musselman, J. L. MacManus-Driscoll, R. H. Friend, D. Di, L. Yang, J. M. Richter, L. Meraldi, D. Credgington, R. H. Friend, R. M. Altamimi, A. Y. Alyamani, K. P. Musselman, *Adv. Mater.* **2017**, *29*, 1605987.
[87] P. H. Sher, C. H. Chen, T. L. Chiu, C. F. Lin, J. K. Wang, J. H. Lee, *J. Phys. Chem. C* **2019**, *123*, 3279.
[88] P. Baronas, G. Kreiza, L. Naimovičius, E. Radiunas, K. Kazlauskas, E. Orentas, S. Juršėnas, *J. Phys. Chem. C* **2022**, *126*, 15327.
[89] X. Chun, S. C. Cheng, X. Lin, V. P. Dravid, Y. W. Chung, Y. Zhu, J. P. Hare, C. L. Reeves, A. K. Cheetham, M. Rühle, H. W. Kroto, M. Walton, R. D., H. Chen, H. S. Yang, G. T. Wu, M. Wang, F. M. Deng, X. B. Zhang, J. C. Peng, W. Z. Li, M. Hines, A. B., G. D. Scholes, G. D. Scholes, M. A. Hines, *Adv. Mater.* **2003**, *15*, 1844.
[90] M. Eich, H. Beisinghoff, R. M. Knodler Ohl, M. Sprave, J. Vydra, M. Eckl, M. Dorr, R. Zentel, M. Ahlheim, M. Stahelin, B. J. Zysset Lidng R Levenson J Zyss, B. C. John de Mello, H. Felix Wittmann, *Adv. Mater.* **1997**, *9*, 230.

© 2025 Wiley-VCH GmbH

21951071, 0, Downloaded from https://advanced.onlinelibrary.wiley.com/doi/10.1002/adom.202500252 by Massachusetts Institute of Technolo, Wiley Online Library on [03/06/2025]. See the Terms and Conditions (https://onlinelibrary.wiley.com/terms-and-conditions) on Wiley Online Library for rules of use; OA articles are governed by the applicable Creative Commons License